Journal of Geodesy manuscript No.
(will be inserted by the editor)

Precise geodesy with the Very Long Baseline Array

Leonid Petrov · David Gordon · John Gipson · Dan MacMillan · Chopo Ma · Ed Fomalont · R. Craig Walker · Claudia Carabajal

the date of receipt and acceptance should be inserted later

Received: 01 June, 2008/ Accepted: tbd

Abstract We report on a program of regular measurements between 1994 and 2007 which used the Very Long Baseline Array and up to 10 additional stations. One of the goals of these sessions was to monitor positions of the array at 1 millimeter level of accuracy and to tie the VLBA into the International Terrestrial Reference Frame. The large number of stations and the many competing goals made scheduling these sessions manually difficult, and lead to advances in scheduling software. We describe the analysis of these data, which is non-standard, and involves translating the data into a form useful for geodetic VLBI. We also describe several interesting geophysical results including measured station displacement due to crustal motion, earthquakes, and antenna tilt. In terms of both formal errors and observed scatter, these sessions are among the very best geodetic VLBI sessions.

Keywords VLBI · coordinate systems · plate tectonics

L. Petrov, D. Gordon, J. Gipson, D. MacMillan
NVI Inc./NASA GSFC, Code 698, Greenbelt, MD 20771 USA
E-mail: Leonid.Petrov@lpetrov.net

E. Fomalont, R. C. Walker
National Radio Astronomy Observatory, 520 Edgemont Rd, Charlottesville, VA 22903–2475, USA

C. Ma
NASA GSFC, Code 698, Greenbelt, MD 20771 USA

C. Carabahal
Sigma Space Corporation, Code 698, Greenbelt, MD 20771 USA

1 Introduction

The method of very long baseline interferometry (VLBI), first proposed by Matveenko (1965), is a technique of computing the cross-power spectrum of a signal digitally recorded at two or more radiotelescopes equipped with independent frequency generators. This spectrum is used in a variety of applications. One of the many ways of utilizing information in the cross-power spectrum is to derive a group interferometric delay (Takahashi et al. 2000; Thompson et al. 2001). It was shown by Shaprio and Knight (1970) that group delays can be used for precise geodesy. The first dedicated geodetic experiment on January 11, 1969 yielded 1 meter accuracy (Hinteregger et al. 1972). In the following decades VLBI technology flourished, sensitivities and accuracies were improved by several orders of magnitude, and arrays of dedicated antennas were built. Currently, VLBI activities for geodetic applications are coordinated by the International VLBI service for geodesy and astrometry (IVS) (Schlüter and Behrend 2007).

Among VLBI dedicated arrays, the Very Long Baseline Array (VLBA) (Napier et al. 1994) of ten 25 meter parabolic antennas stretching over the US territory (Figure 1) is undoubtedly the most productive. The VLBA is a versatile instrument used primarily for astrometry and astrophysical applications. For some of these applications, such as precise parallax measurements, phase referencing for accurate position, phase referencing for detection of weak sources and some others, the positions of reference points of the array elements need to be known with millimeter accuracy.

The use of the Global Positioning System (GPS) can provide very high quality time series of site positions. Averaging GPS data over many years can provide an estimate of the *phase center of a GPS receiver*

with an uncertainty better than one millimeter. However, the use of GPS for measurements of positions of *reference points of the array elements* cannot provide this kind of accuracy. First, measurements of the eccentricity (or tie) vector between the phase center of a GPS receiver and a reference point of a radiotelescope have typical errors of 10–20 mm, according to Ray and Altamimi (2005). Second, systematic errors of the GPS technique, such as phase center variations, multi-path, errors in scale, may cause biases in measurement of the phase center at a level of several centimeters. Therefore, the use of GPS can provide measurements of reference points of array elements with an accuracy of at best 20 mm.

An alternative way for determining antenna reference points is to derive them from dedicated geodetic VLBI observations at the VLBA array. Since the motion of these antenna reference points cannot be predicted precisely, in order to sustain this precision, geodetic observations need to be repeated on a regular basis.

The importance of precise position monitoring was recognized during the development of the VLBA. Between July 1994 and August 2007 132 dedicated 24 hour dual band X/S VLBI sessions under geodesy and absolute astrometry programs with a rate of 6–24 observing sessions per year were carried out. During each session, all ten VLBA antennas and up to 10 other geodetic VLBI stations participated. In this paper we present the geodetic results of this campaign. In section 2 we describe the goals of the observations, scheduling strategies and the hardware configuration. In section 3 we describe the algorithm for computing group delays from the output of the FX VLBA correlator. Validation of post-correlator analysis is presented in section 4. The results and the error analysis are presented in sections 5 and 6. Concluding remarks are given in section 7.

2 Observing sessions

The primary goal of these geodetic VLBI observations was to derive an empirical mathematical model of the antenna reference points motion. This mathematical model can be used for reduction of astronomical VLBA observations as well as for making inferences about the geophysical processes which cause this motion. The second goal was to estimate precise absolute positions of compact sources, not previously observed under absolute astrometry programs, for use as phase referencing calibrators. Other goals, not discussed here, include monitoring a list of $\sim$400 selected sources and producing time series of source coordinate estimates and images for improving the source position catalogue (A. Fey et al. (2008), paper in preparation) and for a study of source structure changes (Piner et al. 2007; Kovalev et al. 2008).

All VLBA antennas have identical designs (Figure 2). They have an alt-azimuthal mounting with an antenna axis offset of 2132 mm. The slewing rate is 1.5° s^{-1} in azimuth and 0.5° s^{-1} in elevation. Permanent GPS receivers are installed within 100 meters of 5 antennas, BR-VLBA, MK-VLBA, NL-VLBA, PIETOWN, SC-VLBA. The system equivalent flux densities (SEFD) of radiotelescopes are in the range of 350–400 Jy when using the dual-frequency S/X system. Observing sessions are typically 24 hours in length. The sources observed are active galactic nuclei at distances of a gigaparsec scale[1] with the continuum radio emission that comes from regions of 0.1–10 mas size.

The VLBA geodetic observations utilized the dual frequency X/S mode, observing simultaneously at S band, centered around 2.3 GHz and at X band, centered around 8.6 GHz. This is enabled by a dichroic mirror permanently positioned over the S band receiver, reflecting the higher frequency radiation towards a deployable reflector leading to the X band receiver. From each receiver four intermediate baseband frequency channels (IFs), each of 4 MHz wide before April 1995 and 8 MHz thereafter, were recorded over a large spanned bandwidth to provide precise measurements of group delays. The sequence of intermediate frequencies was selected to minimize sidelobes in the delay resolution function and to reduce adverse effects of radio interference. The sequence was slightly adjusted over the 14 year period of observations in accordance with changes in the interference environment. The frequency range used in the session of 2007.08.01 is presented in Table 1.

Table 1 The range of intermediate frequencies in the observing session of 2007.08.01, in MHz.

IF1	2232.99 — 2240.99
IF2	2262.99 — 2270.99
IF3	2352.99 — 2360.99
IF4	2372.99 — 2380.99
IF5	8405.99 — 8413.99
IF6	8475.99 — 8483.99
IF7	8790.99 — 8798.99
IF8	8895.99 — 8903.99

[1] 1 gigaparsec $\approx 3 \cdot 10^{25}$ m

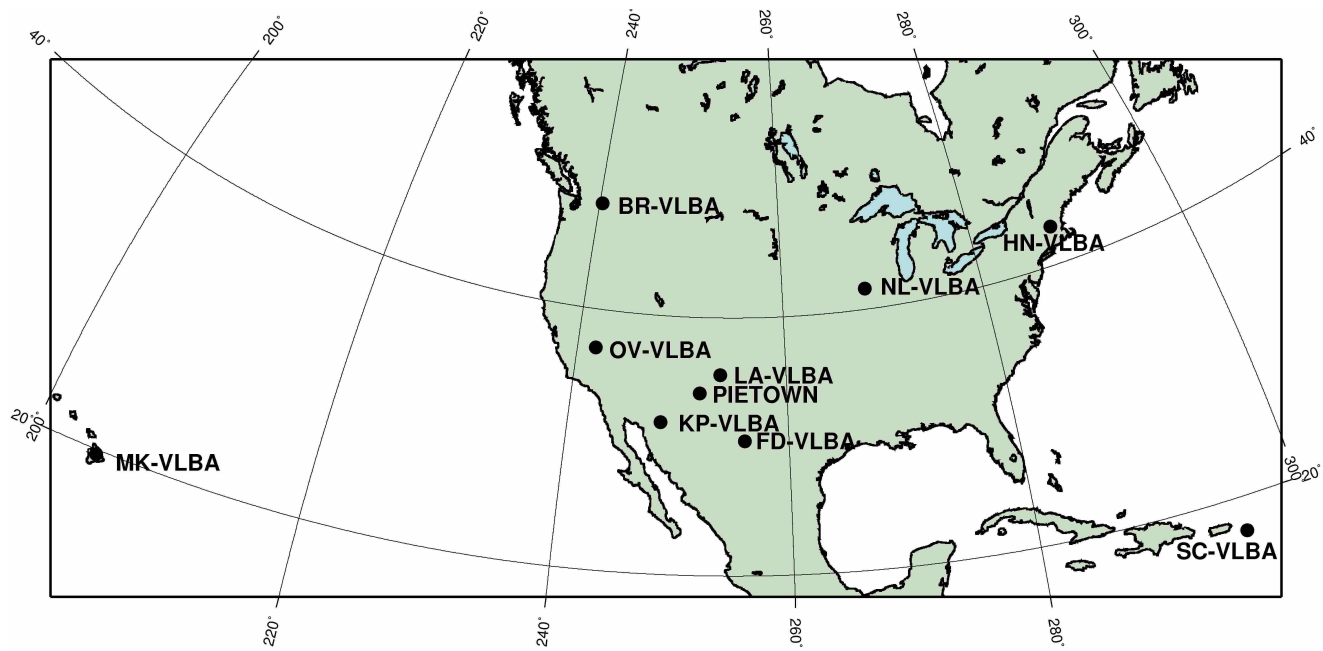

Fig. 1 Positions of the antennas of the Very Long Baseline Array

2.1 Scheduling

Among the 132 observing sessions, 97 can be characterized as global geodetic sessions and 35 can be viewed as absolute astrometry sessions. They differ by scheduling strategy. A wider list of 150–250 sources was observed in each astrometry session while a shorter list of $\sim$100 objects was observed in each geodesy session.

2.1.1 Scheduling of astrometric sessions

Two lists of sources are observed in astrometry sessions: a list of 150–200 target sources and a list of 30–80 tropospheric calibrators. The list of tropospheric calibrator sources is formed using two criteria: a) the compactness at both X and S band, i.e. the ratio at the median correlated flux density at baselines longer than 5000 km to the median correlated flux density at baselines shorter than 900 km, must be greater than 0.5; b) the correlated flux density at baselines longer than 5000 km must be greater than 0.4 Jy at both X and S bands. These sources are frequently observed in other IVS geodetic programs.

Target sources are scheduled to be observed in 1–3 scans in a sequence that seeks to minimize slewing time needed for pointing all antennas of the array to the next source. The scan duration is determined on the basis of the predicted correlated flux density and the SEFDs in such a way that the signal-to-noise ratio (SNR) of the multi-band fringe amplitude will be greater than 20. The scan durations are typically 40–480 s. Usually all antennas of the array observe the same target source during a scan in astrometric schedules.

The sequence of target sources is interrupted every 1.5 hours when 3–5 sources from the list of tropospheric calibrators are observed. The tropospheric calibrators are scheduled in such a way that at each station at least one source is observed in the range $[7, 20°]$ elevations, one sources is observed in the range of $[20°, 50°]$ elevation, and one source is observed above 50° elevation. The purpose of including tropospheric calibrators is a) to estimate reliably the zenith path delay of the neutral atmosphere in the least square (LSQ) solution, and b) to link the positions of rarely observed target sources with the positions of frequently observed calibrators.

Astrometric schedules are prepared with the software package SCHED. The efficiency of these schedules, i.e. the ratio of time on source to the total time of the observing session, is $\sim$70%.

2.1.2 Scheduling of geodetic sessions

Although geodetic VLBI sessions can be scheduled by hand, most geodetic VLBI sessions are scheduled using the automatic mode of program SKED with some subsequent tweaking because of the number of issues involved, e.g., mutual visibility considerations, ensuring adequate sky coverage, minimizing antenna motion, etc. The scheduler instructs the software to schedule ob-

Fig. 2 The VLBA station PIETOWN is in the background. The permanent GPS receiver PIE1 is in the foreground.

servations until some specific time, e.g, 18:30, and the scheduling software SKED automatically does so using a variety of rule-based heuristics to pick the "best" scan at a given time. The scheduling process involves three distinct steps.

1. First, the software constructs a set of scans for further considerations. To a first approximation, this is the set of all possible observations involving the given sources and antennas at a given time. The observations actually considered are limited by so called "major-options". For example, the scheduler can limit the minimum time between observing some sources, which will eliminate the source from consideration. The scheduler can also limit the maximum slew time, which may make a source "invisible" at some antennas.
2. Next, the scans are ranked by their effect on sky-coverage or covariance optimization. For sky coverage, the software finds the distance of a candidate source from all previous sources over some time window, say the last hour. The candidate source with the largest minimum distance from all previous sources has the best sky-coverage. For covariance optimization, the scheduler must first specify parameters to be estimated from the schedule. The scans are ranked by the sum of the formal errors of these parameters. Scans with a lower sum are better. In either case, a subset of the above scans is kept for further consideration. This is typically the highest ranked 40% or 50%.
3. Lastly, the scans are then graded by a further set of "minor options". These include such things as: a) the time to start the scan; b) the time to end the scan; c) distribution of observations by sources; d) distribution of observations by antennas; e) minimizing station idle time; f) optimizing sky coverage; g) optimizing covariance; etc. The scheduler assigns weights to each of these options. The software calculates a score for each option, and then sums the weighted scores to arrive at an overall score for each scan. The scan with the highest score is scheduled. This process is repeated until the end time of the last scan is past the end time specified by the scheduler.

The minor options which are typically used in geodetic VLBA sessions are: 1) `Astro` since we have a set of sources we want to observe a minimum number of times; 2) `EndScan`, which preferentially selects scans which end sooner; 3) `NumObs`, which preferentially selects scans with more observations; 4) `SrcEvn Sqrt`, which tries to even out the distribution of observations; 5) `StatIdle` to minimize station idle time; and 6) `StatWt`, which tries to increase the number of observations of under-observed stations. Some of these options are described in further detail below.

To use the `Astro` option, the scheduler specifies a set of astrometric sources and observing targets expressed as percentages of the total number of observations for the session. These targets can vary on a source by source basis. Typical minimum and maximum targets are 1% and 1.5%, which, for the geodetic VLBA sessions, translates into about 150 to 200 observations. This calculation is done on a running basis, taking into account only those scans already scheduled. Astrometric mode is used to help ensure that we have an adequate number of observations for the monitored sources. If an "astrometric" source has fewer than the minimum number of observations, it will receive a positive score, with a magnitude depending on how far away it is from the target. If it has more than its maximum target, it receives a negative score.

All things being equal, the scheduling software tends to choose strong sources with high-mutual visibility. The `SrcEvn` option was introduced to reduce the disparity in the number of observations between different sources. The `SrcEvn` option has three modes. In all three modes, each source is assigned a target percent-

age of observations. Observations involving sources that are under-observed with respect to their targets are assigned higher scores when ranking scans; observations involving sources which are over-observed are assigned lower scores. 1) In the simplest mode, SKED tries to schedule all sources the same number of times, and the target goal is just `1/Nsrc`, where `Nsrc` is the number of sources. A problem with this approach is that the mutual visibility of sources varies tremendously, with some sources being visible by most of the network most of the time (e.g, circumpolar sources), and other sources, typically low declination sources, being visible only some of the time by some of the antennas. 2) Another approach is to take into account the mutual visibility of sources. For each source, the software generates a series of pseudo-observations spaced 10 minutes apart, for the duration of the schedule. The total number of pseudo-observations is calculated for each source. The observing target is found by dividing the number of pseudo-observations per source by the total number of pseudo-observations. Roughly speaking, the observing targets are what we would get if we chose sources at random from our list. This has the drawback that there can still be large discrepancies between sources with high mutual visibility and those with low. 3) The mode actually used is intermediate between these two. We again calculate the total number of pseudo-observations per source. However, we then take the square root of this number before performing the remaining calculations outlined in mode 2. This mode has the advantage of reducing the disparity between different sources, but doesn't assume that all sources should be observed the same number of times.

For geodetic schedules, it is necessary that there be a sufficient number of observations at each site to estimate parameters of interest, such as station position or Earth orientation, as well as nuisance parameters, such as clocks and atmospheres. One of the problems with geodetic schedules which involve widely dispersed stations is that, because of network geometry, some stations find it easier to observe than others. Because of this we introduced two options to increase the number of observations. The first option, `StatIdle`, calculates the sum of the squares of the idle time for all stations in a scan. Scans with a higher score are preferentially selected for scheduling. The idle time is squared to increase the importance of stations which have not observed recently: i.e, a scan with one station that hasn't observed in 10 minutes should have a higher ranking than one that involves two stations that haven't observed in 5 minutes. The second option is `StatWt`. If this option is turned on, scans involving particular stations, determined by the scheduler, are given higher priority in scheduling.

With the above preliminaries in hand, we turn to an overview of scheduling of geodetic VLBA sessions. The stations involved in an observing session are determined well in advance. The first step in generating the schedules is to choose the sources. A typical geodetic VLBA session has 100 sources. Of these, 0–15 are requested sources, and 30–40 are monitored sources drawn from the pool of ~ 400 objects with the remaining sources drawn from the pool of ~ 100 geodetic sources. The list of monitored sources is generated automatically, based on the observing network and which sources have not been observed recently. Our goal is to schedule each source in our list of monitored sources in at least one session per year. These sources are included in the schedule as "astrometric sources" with initial observing targets of 1–1.5% of the total number of observations. The list of geodetic sources is also automatically generated, being chosen to complement the sky coverage of the monitored sources. Monitored sources and geodetic sources have flux density models adequate for scheduling by SNR. Requested sources usually do not have such a model. They are scheduled "by hand" at VLBA only antennas, usually in two scans each, since the requested sources are usually weak and cannot be detected by the less sensitive geodetic antennas.

Once the sources are picked, the scheduler uses the automatic mode of SKED to generate a series of 24 hour trial schedules. This is done to determine and resolve any issues with the schedule. For example, if a station is under scheduled, the `StatWt` option may be used to increase its number of observations. If some monitored sources are under-observed, their observing targets may be increased. This process may be repeated a few times until the scheduler is satisfied with the results.

Following this, the scheduler generates the final schedule. A session usually starts and ends with two 300 s long scans which are used during correlation for determining clock offsets between the different stations. Following the selection of the initial scan, the scheduler generates the schedule for some block of time, and then inserts scans for some of the requested sources. This process is repeated until the end of the schedule. The scheduler usually concludes the schedule by inserting two final 300 s long scans.

2.2 Session statistics

The distribution of sessions over time is presented in table 2. In each session 7,000–34,000 pairs of X/S group delays were evaluated, for a total of 1,737 947 values.

The ten VLBA stations and 20 other non-VLBA stations took part in the observing campaign, with from 9 to 20 stations in each session. The frequency of station participation in sessions is shown in table 3. Among 4412 observed sources, at least two usable X/S pairs of group delays were determined for 3090 sources.

Table 2 Statistics of VLBA sessions (1) Year, (2) Number of geodetic sessions, (3) Number of astrometric sessions.

(1)	(2)	(3)
1994	3	1
1995	12	2
1996	16	8
1997	6	5
1998	6	0
1999	6	0
2000	6	0
2001	6	0
2002	6	2
2003	6	0
2004	6	4
2005	6	7
2006	7	5
2007	5	1

Table 3 Statistics of observing session per station. (1) IVS station name; (2) geocentric latitude; (3) longitude, positive towards east; (4) Number of observing sessions under geodesy and astrometry with the VLBA array.

(1)	(2)	(3)	(4)
PIETOWN	+34.122	251.880	132
LA-VLBA	+35.592	253.754	130
KP-VLBA	+31.783	248.387	129
BR-VLBA	+47.939	240.316	128
OV-VLBA	+37.046	241.722	128
FD-VLBA	+30.466	256.055	126
HN-VLBA	+42.741	288.013	126
MK-VLBA	+19.679	204.544	124
NL-VLBA	+41.580	268.425	123
SC-VLBA	+17.645	295.416	117
WESTFORD	+42.431	288.511	59
KOKEE	+21.992	200.334	57
GILCREEK	+64.830	212.502	56
ONSALA60	+57.220	11.925	50
WETTZELL	+48.954	12.877	50
MEDICINA	+44.328	11.646	46
NYALES20	+78.856	11.869	38
TSUKUB32	+35.922	140.087	31
HARTRAO	-25.738	27.685	28
GGAO7108	+38.833	283.173	24
TIGOCONC	-36.658	286.974	21
NRAO20	+38.245	280.160	20
MATERA	+40.459	16.704	19
HOBART26	-42.611	147.440	6
KASHIM34	+35.772	140.657	6
ALGOPARK	+45.763	281.927	5
NOTO	+36.691	14.989	4
ZELENCHK	+43.595	41.565	3
SVETLOE	+60.367	29.781	2
URUMQI	+43.279	87.178	1

3 Correlation and post-correlation analysis of observations

Observations at individual stations were recorded on magnetic tapes or (in recent years) on Mark5 disc packs. Cross correlation of the raw data was performed on the VLBA Correlator, in Socorro, N.M, USA. The correlator uses the GSFC program CALC to compute model delays from the geocenter to each station. Each station's bit stream is offset by this correlator model (including clock errors). The resultant correlator output is the amplitudes and residual phases as functions of time (visibility points) for each antenna, referenced to a common point that lays somewhere near the geocenter. Additional processing was required to produce the conventional geodetic/astrometric VLBI observables of group delays and phase delay rates. The details of using the AIPS software package (Greisen 1988) are given in this section. The initial calibrations are:

1. While reading the appropriate raw data into an AIPS data base, small amplitude corrections for the correlator statistics are applied.
2. The reference frequency of the observations is moved from the lower edge to the center of the first IF frequency range. This adjustment lessens the correlation in the determination of the group delay with that of the slightly different peculiar delays for each IF. A corresponding adjustment to the frequency in the AIPS data base is also made.
3. Obviously bad antenna/frequency channels and gross outlier points are flagged.
4. At the VLBA station, relative phase and delay offsets are applied to the visibility points using measured phase calibration tone phases. For all stations, VLBA and non-VLBA, manual phase offsets were also applied, determined by fringe fitting a reference scan on a strong source [2] With a minute or so integration on a strong, compact, radio source, it is possible to determine the relative instrumental phase and residual group delay for each individual IF. These phases are removed from the entire data sets, equivalent to setting the single band and multi-

[2] The non-VLBA stations also had phase calibration systems, but their phases could not be captured in real time, nor could they be extracted during correlation as is done on the Mark 4/5 correlators.

band residual delays to zero at the scan used for the calibration.

The heart of the reduction process is the *fringe fitting* of the data using AIPS task FRING. Each scan (several minutes of data for one source), baseline, frequency band and intermediate frequency channel is processed separately and the following parameters are determined: the average phase at some fiducial time near the center of the scan; the average phase rate with time (fringe rate); and the average phase rate with frequency (single-band delay). A signal-to-noise cutoff of about 3 is generally used in order to omit noisy solutions for relatively weak sources[3].

For those observations in which all of the IF channels in each frequency band (or a designated subset of) have a detection, an AIPS program called MBDLY computes the average phase for the reference frequency and the average phase slope with frequency (so-called, multi-band delay or group delay) that best fits the individual IF phases obtained from FRING. The individual IF solutions for the single-band delay and the fringe rate are averaged over all IF's. Check of the quality of the group delays are obtained by the fringe amplitude SNR, the spread of the individual single-band delays, the fringe rates, and the phase scatter between each measured IF phase versus the best-fit group delay. Observations with large deviations are flagged as low quality and generally are not used in the analysis.

The results from FRING and MBDLY give the phase, single-band delay, fringe-rate, and group delay for a fiducial time near the middle of each observation, baseline and frequency (generally S-band and X-band). These quantities represent the residual values with respect to the correlator model for the observation. When these data are added to that of the correlator model, the results are called the total phase delay, total single-band delay, total fringe-rate and total group delay, respectively. These values are independent of the correlator model, and represent the *observed* delay difference between the radio emission impinging on the two antennas of the baseline at the reference time and frequency.

The correlator model is attached to the AIPS data base. For each source and each antenna, it is represented by a six-order polynomial for every two minute interval, so that its value can be determined at any time with rounding errors below 0.1 ps. The correlator model contains three parts: the geometric delay based on the a priori source position, antenna locations and the a priori Earth orientation parameters, the atmospheric delay based on weather conditions computed by program CALC; and the clock offset determined with the GPS at each individual station. The time-tag associated with the correlator model and the residual parameters is earth-center oriented. That is, the parameters are referenced to the time when the wavefront intercepts a fiducial point chosen to be close to the Earth's center of figure, in order to facilitate the correlation process. The total quantities are then determined by adding the baseline residual parameters to the correlator model difference for the appropriate antenna-pair, interpolated to the scan reference time.

The time-tag convention used in Calc/Solve and most other astrometric software is associated with when the wavefront reaches the reference antenna of the baseline, and can differ by as much as 20 ms from the Earth-centered time-tag. This time-tag is generally shifted to the nearest second of time for convenience.

The AIPS task CL2HF is the software which combines the residual and correlator model quantities, and then changes the time-tag from earth-centered to reference antenna specific. Its output is a so-called 'HF' extension AIPS file which contains the total quantities as well as many other derived quantities needed for Calc/Solve. Some of these quantities are: the quality of the MBDLY fits, various IF frequencies in the session, the angular resolution of the scan and many others. Finally, the AIPS task HF2SV converts the data in the HF extension file to a binary form that is compatible with Mark-3 correlator output that can be later exported to geodetic VLBI databases.

4 Validation of results

Early on, the VLBA/AIPS processed sessions were freely mixed with Mark 4/Fourfit processed sessions, with little noticeable effects. Some effects that were noticed however were 1) the horizontal position of the ONSALA station shifted by approximately 3 mm between the two sets of data, and 2) scatter of source position series for southern sources differed at a level of 0.2–1.0 mas. The shift in ONSALA's position was found to be the result of a strong azimuthal dependence of its phase calibration phases, which showed up because measured phase calibration was not used for ONSALA in the VLBA AIPS processing. The source statistics difference was found to be due to an incorrect accounting in program CL2HF of the total number of bits read from the station tapes at the VLBA correlator. When this was corrected the "southern source" problem disappeared.

A direct comparison of delays and rates processed by the AIPS software package versus the Haystack Fourfit software package was strongly desired. To make such a comparison, the tapes from 8 stations in the rdv22

[3] The AIPS cookbook can be found at `http://www.aips.nrao.edu/cook.html`

VLBA session (2000 July 6–7) were saved and sent to Haystack Observatory. There they were correlated on the Mark 4 correlator and fringed using the HOPS program Fourfit. To minimize the differences in processing, a single set of phase calibration phases was used in both the AIPS and Fourfit processing. Two databases were made of the same baselines processed through the two independent systems, with matching time tags. The regular Calc/Solve analysis was then performed on each to eliminate any bad data points. The observed delays and rates were then differenced and tabulated by baseline. There were constant offsets for each baseline due to differences in single band calibration, and differences in 2π ambiguity shifts. Such delay differences get absorbed into the clock adjustments and do not affect the geodetic or astrometric results. After removal of these constant differences, weighted root mean square (wrms) differences at X-band were computed by baseline. These are given in Table 4. The wrms differences range from as little as 2.5 ps on the KP-VLBA/OV-VLBA baseline, up to 16.1 ps on the BR-VLBA/MK-VLBA baseline. The wrms over all baselines is only 6.0 ps, equivalent to 1.8 mm. By comparison, the average delay formal errors are 7.7 ps on KP-VLBA/OV-VLBA and 17.3 ps on BR-VLBA/MK-VLBA. In a similar comparison between the Mark 3 and Mark 4 correlators and post-processing software at Bonn University, Nothnagel et al. (2002) found an average wrms difference of 21.1 ps on 6 long intercontinental baselines.

Table 4 Rdv22 Correlator Comparisons. A comparison of X-band group delays and phase delay rates between a subset of the rdv22 session processed through the Haystack Mark4 Correlator/Fourfit processing system versus the VLBA Correlator/AIPS processing system.

Baseline	#pts	Length (km)	WRMS Differences Delays (ps)	Rates 10^{-15}
LA-VLBA /PIETOWN	135	237	5.1	31.3
KP-VLBA /PIETOWN	124	417	3.6	14.1
KOKEE /MK-VLBA	169	508	5.1	35.1
KP-VLBA /LA-VLBA	125	652	5.2	15.8
KP-VLBA /OV-VLBA	171	845	2.5	61.1
OV-VLBA /PIETOWN	97	973	7.4	30.0
LA-VLBA /OV-VLBA	76	1088	5.6	22.1
BR-VLBA /OV-VLBA	176	1215	3.3	30.4
BR-VLBA /LA-VLBA	104	1757	3.0	30.3
BR-VLBA /PIETOWN	170	1806	7.8	60.4
BR-VLBA /KP-VLBA	183	1914	6.8	20.8
BR-VLBA /GILCREEK	143	2482	4.0	10.2
GILCREEK/OV-VLBA	24	3584	6.1	51.9
MK-VLBA /OV-VLBA	124	4015	7.4	7.4
KOKEE /OV-VLBA	59	4220	8.4	36.8
GILCREEK/PIETOWN	103	4225	4.8	43.3
GILCREEK/KP-VLBA	98	4322	3.8	9.4
BR-VLBA /MK-VLBA	162	4399	16.1	23.2
KP-VLBA /MK-VLBA	43	4467	13.3	33.2
BR-VLBA /KOKEE	112	4469	9.2	11.3
GILCREEK/KOKEE	95	4728	15.4	36.5
KOKEE /KP-VLBA	113	4736	5.6	24.9
MK-VLBA /PIETOWN	38	4796	9.0	39.7
GILCREEK/MK-VLBA	21	4923	11.6	53.8
LA-VLBA /MK-VLBA	89	4970	9.3	51.1
KOKEE /PIETOWN	105	5040	7.9	77.2
ALL	2859	—	6.0	36.1

5 Analysis

The ionosphere-free linear combinations of dual-frequency group delays are used for parameter estimation using least squares. The differences between observables and theoretical group delays are used in the right hand side of equations of conditions.

Computation of theoretical time delays in general follows the approach outlined in the IERS Conventions (McCarthy and Petit, Eds 2003) and presented in detail by Sovers et al. (1998) with some minor refinements. The expression for time delay derived by Kopeikin and Schäfer (1999) in the framework of general relativity was used. The displacement caused by the Earth's tides were computed using a rigorous algorithm (Petrov and Ma 2003) with a truncation at a level of 0.05 mm using the numerical values of the generalized Love numbers presented by Mathews (2001). The displacements caused by ocean loading were computed by convolving the Greens' functions with ocean tide models using the NLOADF algorithm of Agnew (1997). The GOT00 model (Ray 1999) of diurnal and semi-diurnal ocean tides, the NAO99 model (Matsumoto et al. 2000) of ocean zonal tides, the equilibrium model of the pole tide and the tide with period of 18.6 years were used. The atmospheric pressure loading was computed by convolving the Greens' functions with the output of the atmosphere NCEP Reanalysis numerical model (Kalnay et al. 1996). The algorithm of computations is described in full details in Petrov and Boy (2004).

The a priori path delay in the atmosphere caused by the hydrostatic component was calculated as a product of the zenith path delay computed on the basis of surface pressure using the Saastamoinen (1972a,b) expression and the so-called mapping function (Niell 1996). The mapping function describes the dependence of path delay on the angle between the local axis of symmetry of the atmosphere and the direction to the observed sources. The empirical harmonic variation model `heo_20070802` derived from VLBI observations according to the method proposed by Petrov (2007) was used. Displacement of the reference point of a VLBI

station due to thermal expansion of the antenna was not modeled.

Several solutions were produced. Each solution used the basic parameterization which was common for all runs, and a specific parameterization for an individual solution. Basic parameters belong to one of the three groups:

— *global* (over the entire data set): positions of 3089 sources.
— *local* (over each session): tilts of the local symmetric axis of the atmosphere for all stations and their rates, station-dependent clock functions modeled by second order polynomials, baseline-dependent clock offsets.
— *segmented* (over 0.33–1.0 hours): coefficients of linear spline that models atmospheric path delay (0.33 hour segment) and clock function (1 hour segment) for each station. The estimates of clock function absorb uncalibrated instrumental delays in the data acquisition system.

The rate of change for the atmospheric path delay and clock function between two adjacent segments was constrained to zero with weights reciprocal to $1.1 \cdot 10^{-14}$ and $2 \cdot 10^{-14}$, respectively, in order to stabilize solutions. The weights of observables were computed as $w = 1/\sqrt{\sigma_o^2 + (r(b))^2}$, where σ_o is the formal uncertainty of group delay estimation and $r(b)$ is the baseline-dependent reweighting parameter that was evaluated in a trial solution to make the ratio of the weighted sum of square of residual to their mathematical expectation to be close to unity.

5.1 Baseline analysis

In the preliminary stage of data analysis in addition to basic parameters, we estimated the length of each baseline at each session individually. The purpose of this solution was to determine possible non-linearity in station motion, detect possible outliers, and to evaluate statistics related to systematic errors. The baseline length is invariant with respect to a linear coordinate transformation that affects all the stations of the network. Therefore, changes in baseline lengths are related to either physical motion of one station with respect to another, or systematic errors specific to observations at the stations of the baseline.

We present in figures 3–4 examples of length evolutions for a very stable intra-plate baseline and for a rapidly stretching inter-plate baseline.

As we see, the tectonic motion has shifted station MK-VLBA, located on the fast Pacific plate, by more over 0.5 meters the existence of the array.

Fig. 3 Length of the intra-plate baseline HN-VLBA/FD-VLBA with respect to the average value of 3 623 021.2526 m with the wrms 3.7 mm.

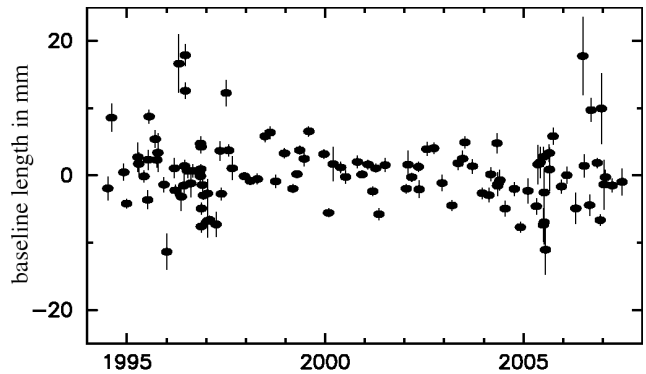

Fig. 4 Length of the inter-plate baseline MK-VLBA/SC-VLBA with respect to the average value of 8 611 584.6972 m with the wrms 9.2 mm.

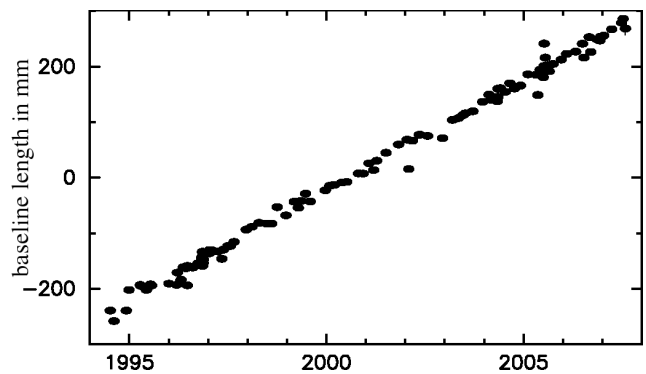

No significant outliers, and no jumps exceeding 1–2 cm were found in examining plots of baseline length evolution. Significant non-linear motion was found only at baselines with station PIETOWN (Figure 5). Analysis of GPS data from the permanent IGS station PIE1 located within 61.9 m from the VLBI station (Figure 2) does not show a similar pattern.

5.2 Global analysis

The purpose of the global solution is to determine the best model of station position motion. In general, the model of motion of the kth station can be represented in this form:

$$\mathbf{r}_k = \mathbf{r}_{ok} + \dot{\mathbf{r}}_k\, t + \sum_{j=1-m}^{m} \mathbf{f}_{ki}\, B_j^m(t) + \sum_i^n \left(\mathbf{h}_{ki}^c \cos(\alpha_i + \omega_i t) + \mathbf{h}_{ki}^s \sin(\alpha_i + \omega_i t)\right) \quad (1)$$

Here $\mathbf{r}_{ok}$ is the position of the station at the reference epoch when t=0, $\dot{\mathbf{r}}_k$ is the linear station velocity,

$B_j^m(t)$ is the B-spline of mth degree with the jth pivotal element. The first two terms in 1 describes the linear station motion, the last one describes harmonic motion, and the third term describes non-linear, anharmonic motion with possible discontinuities caused by seismic events or antenna repair. The epochs of B-spline knots, and the degree of B-spline was determined by analyzing baseline lengths evolution. The model for a non-linear anharmonic motion was applied only to a small number of stations, five of them listed in table 3: PIETOWN due to anomalous motion apparently caused by changes in station tilt, GILCREEK due to seismic and post-seismic motion caused by a Denali earthquake on 2002.11.03, MK-VLBA due to the seismic event on 2007.10.15, and GGAO7108 and MEDICINA due to antenna displacements caused by antenna repairs.

We ran a special global solution, where in addition to parameters estimated in the previous solution, we estimated as global parameters quantities $\mathbf{r}_k, \mathbf{r}_{ok}$ for all stations, quantities $\mathbf{h}^c_{ki}, \mathbf{h}^s_{ki}$ for the stations listed in table 3, and quantities $\mathbf{f}_{ki}$ for five stations.

5.2.1 Required minimum constraints

Equations of light propagation are differential equations of the second order. Their solution does not allow determining specific coordinates of sources and stations, but rather a family of coordinate sets. Boundary conditions should be formulated either implicitly or explicitly in the form of constraints in order to select an element from these sets. These boundary conditions cannot in principle be determined from the observations. Thus, observations alone are not sufficient to evaluate station positions and source coordinates. Coordinates are determined from observations in the form of equations of conditions and boundary conditions in the form of constraint equations.

Expressions for VLBI path delays are invariant with respect to a group of coordinate transformation that involves translation and rotation of site positions at a reference epoch, their first time derivatives, and rotation of source coordinates. In order to remove the rank deficiency, we imposed constraints in the form

$$\begin{aligned} &\sum_k^n (\Delta\mathbf{r}_k \times \mathbf{r}_k)/r^2 = \text{const} \qquad && \sum_k^n \Delta\mathbf{r}_k = \text{const} \\ &\sum_a^q (\Delta\mathbf{s}_a \times \mathbf{s}_a)/r^2 = \text{const} \end{aligned} \tag{2}$$

where $\mathbf{s}_a$ is the coordinate vector of ath source.

The pairs of parameters $\mathbf{r}_{ok}, \mathbf{f}_{ki}$ and $\dot{\mathbf{r}}_k, \mathbf{f}_{ki}$ are linearly dependent, and pairs of parameters $\mathbf{f}_{ki}, \mathbf{h}^c_{ki}$, and $\mathbf{f}_{ki}, \mathbf{h}^s_{ki}$ may be highly correlated depending on frequencies. In order to avoid rank deficiency of a system of equations of conditions, the following decorrelation constraints are to be imposed for each frequency of harmonic constituents:

$$\begin{aligned} &\sum_{k=1-m}^{m-1} f_k \int_{-\infty}^{+\infty} B_k^m(t) \cos\omega_i\, t\, dt = \text{const} \\ &\sum_{k=1-m}^{m-1} f_k \int_{-\infty}^{+\infty} B_k^m(t) \sin\omega_i\, t\, dt = \text{const} \end{aligned} \tag{3}$$

Similar to coordinates, the adjustments of harmonic variations in coordinates are invariant with respect to a group of transformation that involves translation and rotation. In order to remove the rank deficiency associated with this group of transformation, we imposed constraints on estimates of harmonic site position variations as well:

$$\begin{aligned} &\sum_i^n (\mathbf{h}^c_{ki} \times \mathbf{r}_k)/r^2 = \text{const} \qquad && \sum_k^n \mathbf{h}^c_{ki} = \text{const} \\ &\sum_i^n (\mathbf{h}^s_{ki} \times \mathbf{r}_k)/r^2 = \text{const} \qquad && \sum_k^n \mathbf{h}^s_{ki} = \text{const} \end{aligned} \tag{4}$$

In our solutions, we set constants in equations 2–4 to zero.

5.3 Motion of the reference point due to antenna instability

When an antenna is pointed at a source, the actual azimuth and elevation commands sent to the antenna control unit are the expected azimuth and elevation on the sky, including refraction, plus offsets that adjust for imperfections in the antenna and encoders. The offsets typically amount to a few arcminutes. They are calculated using a pointing equation 5 in which the imperfections are parameterized in terms of expected physical effects. The same equation, with site specific values for the coefficients, is used at all VLBA stations. The coefficients for the different effects in equation 5 are determined in pointing observations designed for that purpose.

$$
\begin{aligned}
\Delta\mathrm{Az} = {} & T_e \sin \mathrm{Az} && + T_n \cos \mathrm{Az} \\
& + a_0 && + a_1 \cos \mathrm{El} \\
& + a_2 \sin \mathrm{El} && + a_3 \cos 2\mathrm{Az} \\
& + a_4 \sin 2\mathrm{Az} && + H_a(\mathrm{Az}, \mathrm{El}) \\
\Delta\mathrm{El} = {} & - T_e \cos \mathrm{Az} \sin \mathrm{El} && + T_n \sin \mathrm{Az} \sin \mathrm{El} \\
& + e_0 && + e_1 \cos \mathrm{El} \\
& + e_2 \cos \mathrm{El} && + e_3 \cos \mathrm{El} \sin \mathrm{Az} \\
& + e_4 \cos \mathrm{El} \cos \mathrm{Az} && + e_5 \cos \mathrm{El} \sin 2\mathrm{Az} \\
& + e_6 \cos \mathrm{El} \cos 2\mathrm{Az} && + H_e(\mathrm{Az})
\end{aligned}
\tag{5}
$$

$H_a(\mathrm{Az}, \mathrm{El})$ and $H_e(\mathrm{Az})$ are the contribution to azimuth and elevation offsets due to rail height variations. The rail height H(Az) was determined by leveling for every 3° along the circular rail track of 15.24 m diameter. A three-parameter model $H_o + H_c \cos \mathrm{Az} + \mathrm{H_s} \sin \mathrm{Az}$ was fit to these raw measurements and subtracted. The effect of rail height variations is complicated by the fact that there are 4 wheels, each responding to the rail height at its location and distorting the antenna mount accordingly. A simple model, based on analyses by B. Clark and J. Thunborg (private communication), was developed to describe the effect of rail height:

$$
\begin{aligned}
H_a(\mathrm{Az}, \mathrm{El}) = {} & \\
& h_{a1} \sin \mathrm{El} \left[\mathrm{H}(\mathrm{Az} + 45^\circ) - \mathrm{H}(\mathrm{Az} - 45^\circ)\right] \\
& + h_{a2} \sin \mathrm{El} \left[\mathrm{H}(\mathrm{Az} + 135^\circ) - \mathrm{H}(\mathrm{Az} - 135^\circ)\right] \\
& - h_{a3} \cos \mathrm{El} \left[\mathrm{H}(\mathrm{Az} + 45^\circ) - \mathrm{H}(\mathrm{Az} - 45^\circ)\right] \\
& + h_{a4} \cos \mathrm{El} \left[\mathrm{H}(\mathrm{Az} + 135^\circ) - \mathrm{H}(\mathrm{Az} - 135^\circ)\right] \\
H_e(\mathrm{Az}) \quad = {} & \\
& h_{e1}\ H(\mathrm{Az} + 135^\circ) \\
& + h_{e2}\ H(\mathrm{Az} - 135^\circ) \\
& - h_{e3}\ H(\mathrm{Az} + 45^\circ) \\
& - h_{e4}\ H(\mathrm{Az} - 45^\circ)
\end{aligned}
\tag{6}
$$

It should be noted that the eight coefficients h_{a1}—h_{a4} and h_{e1}—h_{e4} are linearly dependent. The equations 6 can be reduced to linear combinations of two independent parameters. Since all VLBA antennas have identical design, these parameters are considered to be the same for all antennas. They were determined for several antennas with the largest rail height variations and then kept fixed. The method is described in details by Walker (1999).

The parameters of the pointing equation 5, T_e, T_n, a_0–a_5, e_0–e_6 are determined using least squares fits to measurements of residual pointing offsets. These measurements are made at 13 observing bands right after the weekly maintenance day, during "startup" observations designed to help verify proper operation of the telescope. Special targeted pointing observations, often of order 10 hours in length, are made during other times that the antennas are not needed for interferometer observations. These special observations often concentrate on the 22 GHz and 43 GHz bands.

Such measurements are made by recording the total power output in baseband channels of 16 MHz bandwidth attached to both left and right circular polarization output from the receiver while pointing at each of 10 positions near the expected position of a strong source. The 10 points are off-source, half-power, on-source, half-power, off-source in azimuth, then in elevation, with the two half-power and off positions being on opposite sides of the source. The off positions are about 6 beam half-widths from the source, but, for the elevation pattern, much of that offset is in azimuth to allow even steps in elevation. The FWHM of the beam at 22 GHz is $1'.9$. The residual pointing offset, and gain, are determined by subtracting interpolated off-source powers from the on-source and half-power number, and then fitting for a peak amplitude and position. The even steps in elevation of the elevation scan make the removal of gradients in elevation, such as naturally arise from the atmosphere, more effective.

Throughout this process, a modulated noise calibration signal of known equivalent temperature is injected in front of the receiver amplifiers and synchronously detected along with the total power. This allows the total power and the power contributed by the target source to be calibrated in terms of antenna temperature. Some of the sources observed are of known flux density so the gain, as a ratio of source flux density to antenna temperature, can be determined. Continuum sources used for pointing observations must be stronger than 5 Jy to provide enough power so that they are not masked by normal atmospheric fluctuations.

Occasionally, all pointing observations made over the course of about three months are gathered together for a single fit. Such an analysis typically involves about 1000 separate measurements at each of the 22 GHz and 43 GHz bands. The high frequency bands are used to determine most of the pointing equation parameters because, with their smaller beam widths, they produce more accurate pointing residual measurements.

Prior to a fit, the effects of beam squint are removed. This is the offset between the left and right circular polarized beams caused by the asymmetric geometry of the VLBA antennas. Since antennas always point to a position half way between the right and the left circular polarization beams regardless of the polarization being observed, it is always pointed a bit off from the source position.

In the fit for the pointing parameters, some of the terms described above are held fixed. The axis non-

perpendicularity, a_2 is generally held to be zero. Also, some terms in the pointing equation are highly correlated so, while the overall equation will be a good description of the required pointing offsets, not too much should be made of variations of the individual items of the correlated sets. An example would be the constant, sin(El), and cos(El) terms in the elevation equation which have to be determined from data that only span about 75 deg in elevation. The terms, T_e, T_n, give the east and north tilts of the fixed azimuthal axis. They depend on sin(Az) and cos(Az) with full coverage of azimuth are not significantly correlated with other terms. A classic example of tilt is the leaning town in Pisa. The tilt can be considered as a rotation of the antenna with respect to a certain point. This rotation shifts the position of the reference point, the projection of the elevation axis on the azimuthal axis. This displacement also affects the position of the antenna.

Fig. 5 Length of the inter-plate baseline LA-VLBA/PIETOWN with respect to the average value of 417 009.1252 m. The baseline length estimates exhibit a non-linear motion caused by variations in the antenna's tilt.

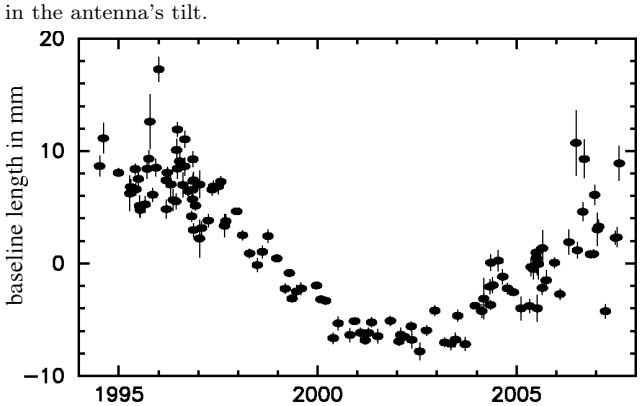

The time series of length estimates at baselines with PIETOWN show a significant systematic behavior. It turns out that these anomalous baseline length variations can be almost entirely explained by variations of the tilt of the PIETOWN antenna. We have derived an empirical model of station position variations by estimating the B-spline coefficients, and derived an empirical time series of PIETOWN displacements using this mode. The time series of the horizontal site displacements was fit to the north and east tilt measurements time series. The adjusted parameter is 20.5±0.2 m. Its physical meaning is the length between the center of the antenna rotation and the antenna reference point. As Figures 6 show, the empirical model of site displacement is in agreement with tilt measurements within its formal uncertainties, at a 0.5 mm level. The site position series of the nearby GPS station PIE1 located at a distance of 61.8 m from the VLBI antenna shows (Figures 7) some similarity in non-linear motion in the north component, but no similarity in the east component. The origin of the non-linear motion of PIETOWN is not clear.

5.3.1 Analysis of the VLBA array velocity field

Since station velocity estimates depend not only on observations but on constraint equations with an arbitrary right hand side, the estimates of motion of the VLBA array as a whole is also arbitrary. This means that all velocity vectors of the network can be transformed as

$$\mathbf{v}_n = \mathbf{v}_o + \widehat{\mathcal{M}}\,\mathbf{s} \tag{7}$$

where $\widehat{\mathcal{M}}$ is the transformation matrix, and $\mathbf{s}$ is an arbitrary 6-vector of translation-rotation:

$$\widehat{\mathcal{M}} = \begin{pmatrix} 1 & 0 & 0 & 0 & r_3 & -r_2 \\ 0 & 1 & 0 & -r_3 & 0 & r_1 \\ 0 & 0 & 1 & r_2 & -r_1 & 0 \end{pmatrix} \tag{8}$$

$$\mathbf{s} = (\,T_1\;\; T_2\;\; T_3\;\; \Omega_1\;\; \Omega_2\;\; \Omega_3\,)^\top$$

We can find such a vector $\mathbf{s}$ that the transformed velocity field would have some desirable properties. That is equivalent to running a new solution with different constants in the right hand side in constraint equations 2–4.

In order to address the question of stability of the array, we would like to learn which part of the array, if any, exhibits only a rigid horizontal motion, i.e. their relative horizontal velocities are close to zero.

Equation 9 is transformed to a local topocentric coordinate system of the ith station by multiplying it by the rotation matrix P:

$$\widehat{\mathcal{P}}_i \widehat{\mathcal{M}}_i\,\mathbf{s} = \mathbf{u}_i - \widehat{\mathcal{P}}_i\,\mathbf{v}_{oi} \tag{9}$$

where $\mathbf{u}$ is the vector of the station velocity in a topocentric coordinate system after the transformation. We can find vector $\mathbf{s}$ from equation 9 if we define $\mathbf{u}_i$ according to the model of rigid motion. We split the set of stations into two subsets. The first set called "defining" exhibits only rigid motion, either horizontal or vertical, or both. Stations from the second set called "free" have non-negligible velocities with respect to the rigid motion.

We pick equations 9 for horizontal components of defining stations for horizontal motion, set these components of vector $\mathbf{u}_i$ to zero, and build a system of linear equations. This system is augmented by adding equations for the vertical components of defining stations for vertical motion and also setting these components of vector $\mathbf{u}_i$ to zero.

Fig. 6 Nonlinear motion of station PIETOWN as estimated from global VLBI analysis (smooth line) and changes in the tilt converted to displacement of the antenna reference point, considering rigid rotation of the antenna. The shadow shows the 1-σ formal uncertainties of the displacement estimate.

a) East component b) North component

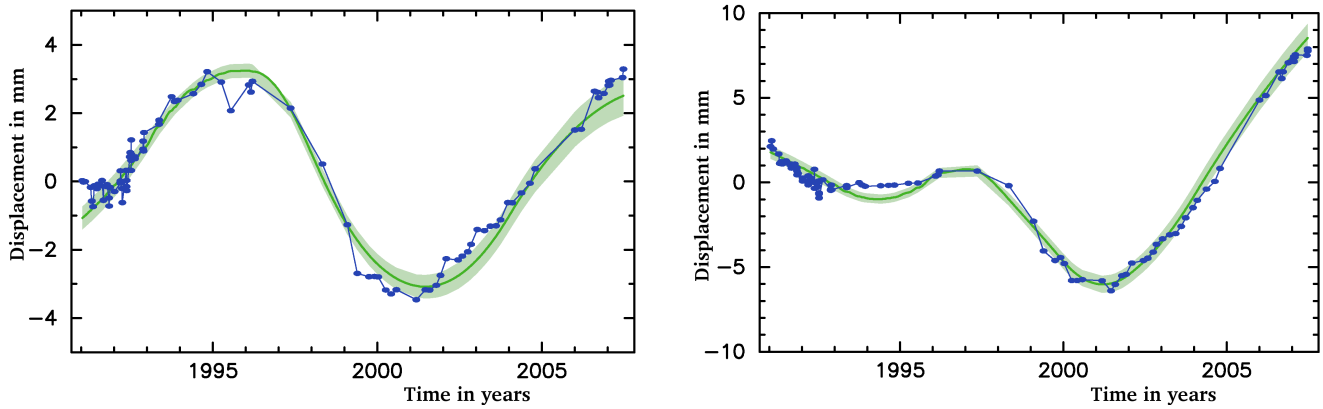

Fig. 7 Nonlinear motion of station PIE1 as estimated from GPS time series after subtracting the mean position, linear velocity, annual and semi-annual position variations from the LSQ fit of daily estimates of station positions generated by JPL (M. Heflin, 2007, personal communication) and subsequent smoothing.

a) East component b) North component

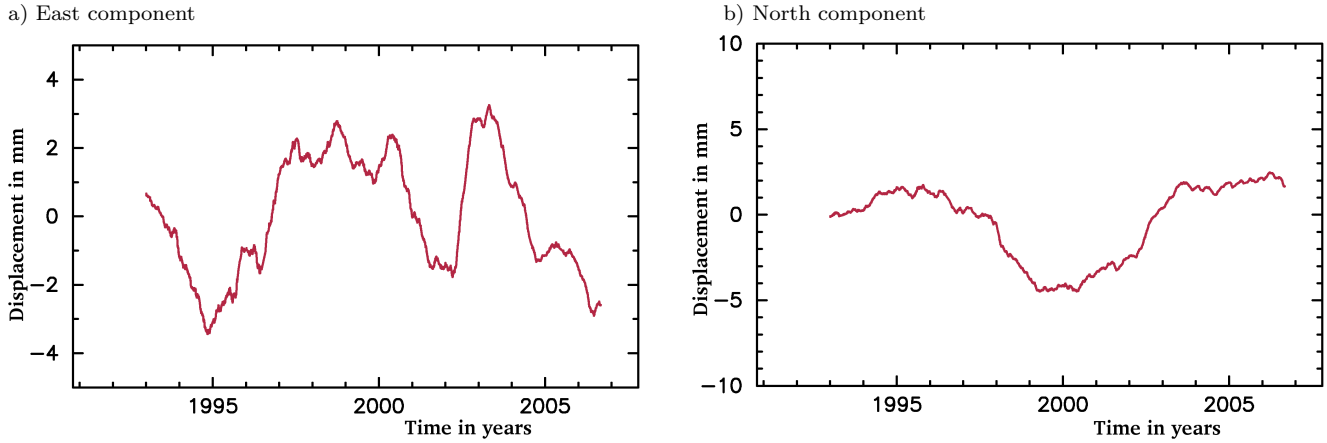

When the number of equations exceeds 6, the system becomes redundant. We solve it by LSQ with a full weights matrix $\widehat{\mathcal{W}}$:

$$\widehat{\mathcal{W}} = \left(\widehat{\mathcal{P}}_a \operatorname{Cov}(v, v^\top)\, \widehat{\mathcal{P}}_a^\top + \widehat{\mathcal{A}}\right)^{-1} \tag{10}$$

where $\widehat{\mathcal{P}}_a$ is a block-diagonal matrix formed from matrices $\widehat{\mathcal{P}}_i$, $\widehat{\mathcal{A}}$ is a diagonal reweighting matrix with an additive correction to weights. Values $(0.4\,\mathrm{mm/year})^2$ for both horizontal and vertical components of velocities were used in the matrix $\widehat{\mathcal{A}}$ in our solution.

We extended our analysis to four non-VLBA stations located in the vicinity of VLBA antennas. The set of defining stations was found by an extensive trial. The residual velocity of defining stations with respect to the rigid motion was examined. We found a set of 7 defining stations for which the residual velocity does not exceed 2σ.

Then, transformation 9 and the rotation to the local topocentric frame were applied to both defining and free stations. The covariance matrix for velocity estimates of free stations was computed as:

$$\begin{aligned}\operatorname{Cov}(v_n, v_n{}^\top) = {} & \widehat{\mathcal{P}}_a \operatorname{Cov}(v_o, v_o{}^\top)\widehat{\mathcal{P}}_a^\top + \\ & \widehat{\mathcal{P}}_a \widehat{\mathcal{M}} \operatorname{Cov}(s, s^\top)\widehat{\mathcal{M}}^\top \widehat{\mathcal{P}}_a^\top\end{aligned} \tag{11}$$

and for defining stations as

$$\begin{aligned}\operatorname{Cov}(v_n, v_n{}^\top) = {} & \widehat{\mathcal{P}}_a \operatorname{Cov}(v_o, v_o{}^\top)\widehat{\mathcal{P}}_a^\top + \\ & \widehat{\mathcal{P}}_a \widehat{\mathcal{M}} \operatorname{Cov}(s, s^\top)\widehat{\mathcal{M}}^\top \widehat{\mathcal{P}}_a^\top + \\ & \widehat{\mathcal{P}}_a \operatorname{Cov}(s, s^\top)\widehat{\mathcal{M}}\widehat{\mathcal{W}} \operatorname{Cov}(v_o, v_o{}^\top)\widehat{\mathcal{P}}_a^\top + \\ & \widehat{\mathcal{P}}_a \operatorname{Cov}(v_o, v_o{}^\top)\widehat{\mathcal{W}}\widehat{\mathcal{M}}^\top \operatorname{Cov}(s, s^\top)\widehat{\mathcal{P}}_a^\top\end{aligned} \tag{12}$$

The latter expression takes into account statistical dependence of the old velocity $\mathbf{v}_o$ and the vector $\mathbf{s}$.

The results are presented in table 5. It is remarkable that there exists a set of 6 stations spread over distances

Table 5 Station local topocentric velocities with respect to the rigid North American plate. Units: mm/yr. The quoted uncertainties are re-scaled 1-σ standard errors. Last column indicates whether the station was used as defining for horizontal (h) or vertical (v) motion of the plate.

Station	Up	East	North	Def
BR-VLBA	0.0 ± 0.1	1.9 ± 0.3	-0.3 ± 0.4	v
FD-VLBA	1.2 ± 1.0	0.4 ± 0.2	-0.1 ± 0.2	h
HN-VLBA	0.2 ± 0.3	-0.1 ± 0.2	-0.1 ± 0.2	hv
KP-VLBA	2.3 ± 1.0	-0.2 ± 0.2	0.1 ± 0.2	h
LA-VLBA	1.3 ± 0.8	0.0 ± 0.3	0.0 ± 0.2	h
MK-VLBA	0.9 ± 1.1	-55.0 ± 1.4	52.5 ± 1.1	
NL-VLBA	-1.1 ± 0.5	0.0 ± 0.2	0.1 ± 0.3	h
OV-VLBA	2.0 ± 0.8	-6.0 ± 0.3	5.0 ± 0.4	
PIETOWN	2.1 ± 0.9	-0.4 ± 0.3	-1.5 ± 0.3	
SC-VLBA	-1.2 ± 1.2	19.0 ± 0.8	5.3 ± 0.4	
GILCREEK	3.0 ± 1.4	4.0 ± 0.6	-10.2 ± 0.7	
GGAO7108	-0.9 ± 0.5	-0.4 ± 0.3	-0.5 ± 0.3	
KOKEE	2.7 ± 1.0	-54.3 ± 1.3	52.9 ± 1.2	
WESTFORD	-0.3 ± 0.3	-0.1 ± 0.2	0.0 ± 0.2	hv

of 1–3 thousand kilometers with an average residual horizontal velocity of only 0.2 mm/yr.

5.3.2 Detection of post-seismic deformations

On 2006.10.15 two powerful earthquakes struck the Island of Hawaii. The magnitude 6.7 event that occurred at 17:07:48 UTC was located 16 km North-Northwest of Kailua Kona, a town on the West coast of the Big Island of Hawaii (19°.820 N, 156°.027 W), in the Kiholo Bay, 38 km beneath the surface. The Kiholo Bay event was followed by a magnitude 6.0 Makuhona event 7 minutes later, located 44 km north of the airport and at 20 km depth. The epicenter is shown in Figure 8.

According to the USGS, there were about 80 shallow, lower magnitude aftershocks recorded in the following 24 hours, the largest one having a magnitude of 4.2, at 20:35 UTC the same day. Although the two major events were only 7 minutes apart, their depth difference and aftershock epicenters suggest that the 6.0 event may not have been an aftershock of the larger event, and that they have different sources. There were no reported fatalities, but electric power was lost statewide shortly after the event. Despite its moderate depth, the earthquake generated high accelerations in the epicentral region, with strong ground motions which lasted for approximately 20 s during the Kiholo Bay event, and 15 s during the Mahuhona event. One station northeast of the epicenter recorded a max horizontal component of 1.03 g peak acceleration.

The largest historical earthquakes in Hawaii have occurred beneath the flanks of Kilauea, Mauna Loa and Hualalai volcanoes, when stored compressive stresses from magma intrusions into their adjacent rift zones are released. Their sources are related to near-horizontal

Fig. 8 Map of the Hawaii Island. Location of seismic events on 2006.10.15 is shown with asterisk. The arrows show site displacement caused by these events from analysis of VLBI observations (bottom) and GPS observations (up).

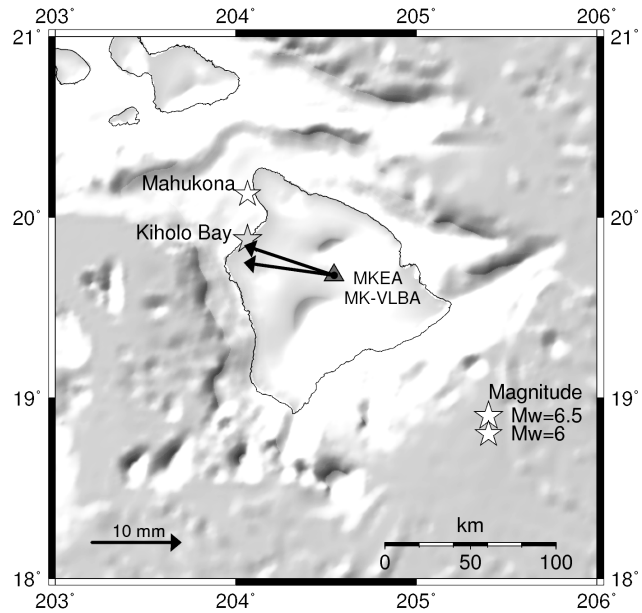

basal decollements at approximately 10 km, separating the emplaced volcanic material from the older oceanic crust. The Kiholo Bay event was considered a tectonic event, occurring on a normal fault and not volcano-related, probably reflecting the long term accumulation and release of lithospheric flexural stresses caused by the island-building process. Deeper, 30–40 km deep, earthquakes like this result from a long-term geologic response to flexural fracture of the underlying lithosphere from the load of the island mass (Chock 2006).

The distance from the epicenter to the MK-VLBA station is 62 km. No structural damage was reported. As a response to the event, an additional observing session was added to the schedule on 2006.11.08 in order to detect possible post-seismic deformation. Preliminary analysis early in 2007 did not find any position changes exceeding 1 cm.

Later, we reanalyzed the dataset and parameterized non-linear motion with the B-spline of the zeroth degree with two knots: at 1994.07.08 (beginning observations) and 2006.10.15 17:07:48. Using these two estimates of B-spline coefficients and their covariance matrices, we have computed the displacement vector:

$$\begin{aligned} \text{Up} &= -7.7 \pm 1.3 \quad \text{mm} \\ \text{East} &= -10.0 \pm 0.4 \quad \text{mm} \\ \text{North} &= 1.5 \pm 0.4 \quad \text{mm} \end{aligned}$$

where the quoted uncertainties are unscaled 1-σ formal errors. The vertical and west displacement looks

very significant. However, the presence of outliers may cause an artificial jump and various systematic correlated errors may cause estimates of uncertainties to be unreliable.

In order to check the robustness of the solution we performed two tests. Can they be caused by the noise in the data or systematic errors unrelated to physical station displacement? In the first test we ran two solutions. In the first run we deselected every even observation at baselines with MK-VLBA, and in the second run we deselected every odd observation. Each solution used 1/2 of the independent observations. The difference in estimates of the displacement was 0.14 mm in the vertical component and 0.06 mm in the horizontal component. This test checks the contribution of random errors uncorrelated at time scale of the interval between observations, typically 5–10 minutes.

In the second test we made 21 trial solutions which differed only by epochs of the B-spline knots. In each trial solution we shifted the epoch of the knot six months backward with respect to the previous. The procedure for computing theoretical path delay for these trial solutions incorporated the estimate of the displacement at 2006.10.15 17:07:48 epoch from the initial solution. The rms of time series of displacement estimates at epochs with no reported seismic events were 2.1 mm for the vertical component and 1.3 mm for the horizontal component of the MK-VLBA displacement vector. We consider these statistics as a measure of the robustness of the estimates of the displacement vector. Both tests support our claim that VLBI observations detected a displacement of station MK-VLBA caused by the seismic event at 2006.10.15 at the confidence level of 99.5%.

Since there is a GPS receiver named MKEA located 88 meters from the VLBA station MK-VLBA, we examined the GPS site motion series to determine the corresponding co-seismic offset. For the analysis, we used the MKEA daily position time series generated by JPL (M. Heflin, 2007, personal communication). We obtained the following estimate for the co-seismic displacement vector:

$$\begin{aligned} \text{Up} &= -6.3 \pm 0.9 \quad \text{mm} \\ \text{East} &= -9.9 \pm 0.4 \quad \text{mm} \\ \text{North} &= 3.5 \pm 0.2 \quad \text{mm} \end{aligned}$$

Here, the uncertainties are unscaled 1-sigma formal errors. This is reasonable because the position repeatabilities computed from the position time series are close to the formal uncertainties of the daily estimates. The VLBI and GPS vertical and east displacements are consistent within their 1-sigma error bars but the 2 mm difference in the north displacement is too large to be explained by the formal uncertainties.

Table 6 Amplitudes of vertical component of harmonic variations of VLBA station positions in mm.

Station	annual	semi-annual	diurnal	semi-diurnal
BR-VLBA	8.0 ± 0.3	3.3 ± 0.3	1.0 ± 0.2	0.5 ± 0.2
FD-VLBA	1.8 ± 0.3	1.8 ± 0.3	0.4 ± 0.2	1.5 ± 0.2
HN-VLBA	5.4 ± 0.3	2.3 ± 0.3	1.5 ± 0.3	1.0 ± 0.3
KP-VLBA	1.7 ± 0.3	1.8 ± 0.3	0.2 ± 0.2	0.8 ± 0.2
LA-VLBA	1.0 ± 0.3	3.2 ± 0.2	1.3 ± 0.2	0.9 ± 0.2
MK-VLBA	2.5 ± 0.4	2.5 ± 0.4	0.8 ± 0.3	2.5 ± 0.3
NL-VLBA	4.1 ± 0.3	3.6 ± 0.3	0.8 ± 0.2	0.2 ± 0.2
OV-VLBA	2.7 ± 0.3	2.0 ± 0.3	1.1 ± 0.2	0.9 ± 0.2
PIETOWN	1.8 ± 0.3	0.8 ± 0.3	1.1 ± 0.2	1.2 ± 0.2
SC-VLBA	2.6 ± 0.5	3.0 ± 0.5	0.5 ± 0.4	1.3 ± 0.4

Table 7 Amplitudes of horizontal component of harmonic variations of VLBA station positions in mm.

Station	annual	semi-annual	diurnal	semi-diurnal
BR-VLBA	0.8 ± 0.1	0.3 ± 0.1	0.3 ± 0.1	0.2 ± 0.1
FD-VLBA	1.4 ± 0.1	0.1 ± 0.1	0.2 ± 0.1	0.1 ± 0.1
HN-VLBA	0.9 ± 0.1	0.2 ± 0.1	0.2 ± 0.1	0.1 ± 0.1
KP-VLBA	1.5 ± 0.1	0.3 ± 0.1	0.4 ± 0.1	0.2 ± 0.1
LA-VLBA	1.1 ± 0.1	0.3 ± 0.1	0.3 ± 0.1	0.1 ± 0.1
MK-VLBA	0.8 ± 0.2	0.4 ± 0.2	0.8 ± 0.1	0.3 ± 0.1
NL-VLBA	0.7 ± 0.1	0.2 ± 0.1	0.2 ± 0.1	0.2 ± 0.1
OV-VLBA	1.2 ± 0.1	0.2 ± 0.1	0.5 ± 0.1	0.3 ± 0.1
PIETOWN	1.5 ± 0.1	0.2 ± 0.1	0.3 ± 0.1	0.3 ± 0.1
SC-VLBA	0.7 ± 0.2	0.9 ± 0.2	0.4 ± 0.1	0.3 ± 0.1

5.3.3 Harmonic variations in site positions

The technique of estimation of harmonic variations in site positions directly from analysis of group delays was developed by Petrov and Ma (2003). The purpose of estimation of the harmonic site position variations was to remove the remaining mismodeled harmonic non-tidal signal. We estimated sine and cosine amplitude of variations in all three components of site position vector at annual (Sa), semi-annual (SSa), diurnal (S_1), and semi-diurnal (S_2) frequency for all VLBA and 35 other non-VLBA stations. The seasonal signal is caused by unaccounted hydrology loading, by the modulation of systematic errors in troposphere path delay, and possibly some other effects. Sun-synchronous diurnal variations can be caused by thermal variations, by the modulation of systematic errors in troposphere path delay, or unmodeled non-tidal loading.

In order to evaluate the robustness of the estimates at low frequencies we performed two tests. In the first test we split each session into two equal subsets, one with odd observations, another with even observations, and processed both subsets separately. We examined the differences in estimates of sine and cosine amplitudes and compared then with formal uncertainty of estimates. The differences are within 1-sigma formal uncertainty. Formal uncertainties of VLBI site positions

are in the range 0.2–0.5 mm for the horizontal component and 0.6–1.0 mm for vertical components.

We also estimated site position variations at a frequency of $2.5 \cdot 10^{-7}$ rad s^{-1} that corresponds to a period of 0.8 year where no harmonic signal is expected. The average amplitude of the vertical displacement over the ten VLBA stations is 1.2 mm, and the average amplitude of horizontal displacement is 0.2 mm. These estimates should be considered as the upper limit of uncertainties, since the observed harmonic signal at frequency $2.5 \cdot 10^{-7}$ rad s^{-1} is affected by both systematic errors and real displacements at this frequency, caused by anharmonic, broad-band site position displacements.

We see that the combined contribution of seasonal position variation, unaccounted for in the theoretical model, can reach 1 cm for the vertical component of VLBA stations and 1.5 mm for the horizontal component and is statistically significant for most of the stations at the 95% confidence level. Unaccounted diurnal position variations are at the level of 1–2 mm.

6 Error analysis

Uncertainties of estimated parameters can be evaluated using the law of error propagation, provided the unmodeled contribution to group delay is due to random uncorrelated errors with known variance. The parameter estimation procedure provides estimates of these errors based on the SNR of group delays. These errors are labeled as formal errors and they are considered as lower limits of actual errors. Formal uncertainties of site position estimates of VLBA stations are in the range of 0.5–1.0 mm for vertical components and 0.2–0.5 mm for horizontal components. Formal uncertainties of VLBA site velocity estimates are in the range of 0.07–0.1 mm/yr for vertical components and 0.04–0.05 mm/yr for horizontal components.

Many factors contribute to increase of errors. Among them are underestimated uncertainties of group delays due to phase instability of the data acquisition system, unmodeled instrumental errors, unaccounted atmospheric fluctuations, correlations between observations, and unaccounted environmental effects.

Another measure of accuracy is a decimation test. We ran two special solutions and excluded every second observation, odd or even, at VLBA stations. The two datasets have independent *random* errors. The root mean square of differences between estimates from these solutions divided by $\sqrt{2}$ provides a measure of accuracy that is independent of estimates of the uncertainty of each individual observation. However, many other factors that affect results, such as mismodeled delay in the neutral atmosphere, are common in the two subsets. We ran another decimation test and used every second observing session. In the first test, matrices of equation of conditions were almost identical, but the data were affected by the same systematic errors. In the second test, the systematic errors were less common, but the matrices of equations of conditions have greater differences.

Table 8 Formal uncertainties and rms of differences of two decimation tests for estimates of site positions and site velocities. The estimates are given for horizontal and vertical components separately.

Statistics	Position mm		Velocity mm/yr	
	v	h	v	h
Formal σ	0.7	0.3	0.11	0.04
Observation decimation	0.3	0.06	0.04	0.02
Session decimation	1.4	0.3	0.09	0.06

The differences are given in Table 8. In the absence of systematic errors both decimation solutions would give close results. Analysis of the statistics shows significant discrepancies between the decimation solutions. Estimates of site positions and velocities in solutions where every second observation is removed are a factor of 2–3 closer to each other than in solutions where every second session is removed. This is an indication that systematic errors on the time scale of several minutes — the typical time between observations — are correlated. The session decimation test suggests that the vertical site position errors should be rescaled by a factor of 2. This rescaling may be related to unaccounted errors in modeling the contribution of the neutral atmosphere.

We estimated Earth Orientation parameters (EOP) in our solution. Comparison of our EOP estimates with independent GPS time series `igs00p03.erp`[4] gives us another measure of the accuracy of our results. We computed the rms of differences in pole coordinates for sessions in astrometric mode and sessions in geodetic modes. Only sessions after 1997 were used for this comparison, since GPS estimates prior to this date are not very accurate. As we see from Table 9 the VLBA estimates of pole coordinates from geodetic observations are approximately as close to GPS results as regular IVS sessions. However, the EOP from astrometric sessions divert from the GPS time series by a factor of 2 greater than the EOP from geodetic VLBI sessions.

The baseline length repeatability test provides another measure of solution accuracy. For each baseline a series of lengths was obtained. Empirical non-linear site position variations described above were applied as a priori. A plot of the baseline length repeatability of

[4] Available at ftp://cddisa.gsfc.nasa.gov/gps/products/igs00p03.erp.Z

Table 9 The rms of differences in pole coordinates estimates between the VLBI results and the GPS time series `igs00p03.erp`. Only data after 1997.0 are used. Comparison is made separately for VLBA sessions in astrometric mode (only 10 VLBA stations) and VLBA sessions in geodetic mode (10 VLBA stations plus 3–10 non-VLBA stations).

Sessions	X-pole	Y-pole
VLBA, Astrometric mode	0.87 nrad	1.15 nrad
VLBA, Geodetic mode	0.54 nrad	0.43 nrad
IVS sessions in 2006–2007	0.39 nrad	0.47 nrad

VLBA baselines is presented in figure 9. For comparison, baseline length repeatability at non-VLBA baselines is also shown.

Fig. 9 Baseline length repeatability as a function of baseline length. Solid disks shows estimates of baseline length repeatability between VLBA sites, circles shows repeatability between non-VLBA sites.

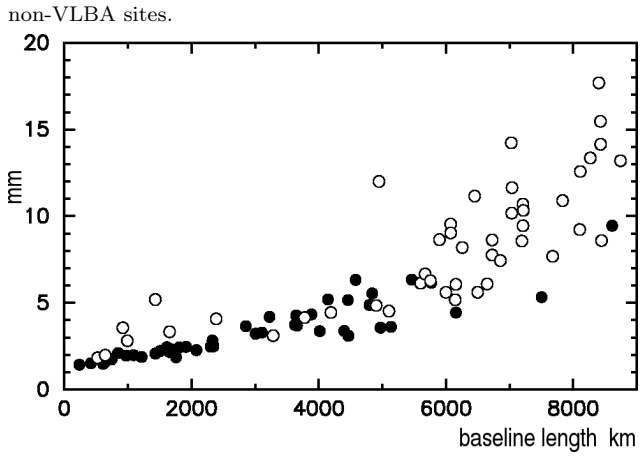

A linear model of baseline lengths was fit to each series, and the wrms of the deviations from the linear model, the baseline length repeatability, was computed for each baseline. The plot of baseline length repeatability shows that the scatter in baseline lengths estimates between VLBA sites is less than the scatter in baseline length between dedicated geodesic VLBI stations. The set of wrms was fit by a function $\sqrt{A^2 + (B \cdot L)^2}$ where L is the mean baseline length. Coefficients A and B, which represent the average baseline length repeatability, are a measure of accuracy. For the VLBA baselines, A = 1.6 mm, B=0.9 ppb, for non-VLBA baselines A=2.0 mm, B=1.4 ppb. Growth of the baseline length repeatability with the baseline length reflects the contribution of the unmodeled path delay in the neutral atmosphere that affects the vertical component of site position stronger than the horizontal one.

The results of error analysis allows us to draw the conclusion that the errors of predicted site positions for any epoch within the time range of observations, [1994, 2008], are within a 2–3 mm range for the vertical component and 0.4–0.6 mm for the horizontal component. The predicted positions, based on the adjusted parameters of the site motion model, includes mean site positions at the reference epoch, site velocities, coefficients of the harmonic and B-spline models. The estimates of errors for the vertical coordinates were derived from the formal errors by inflating by a factor of 2, as a session decimation test suggests. Provided that there is no future motion other than harmonic position variations and linear velocities happens, and no seismic events, or unmodeled variable tilt, by 2020 the error in site position predictions will grow by a factor of 2 (refer to Figure 10).

Fig. 10 Errors of prediction of MK-VLBA vertical coordinate. The errors were inflated by a factor of 2 with respect to the formal errors.

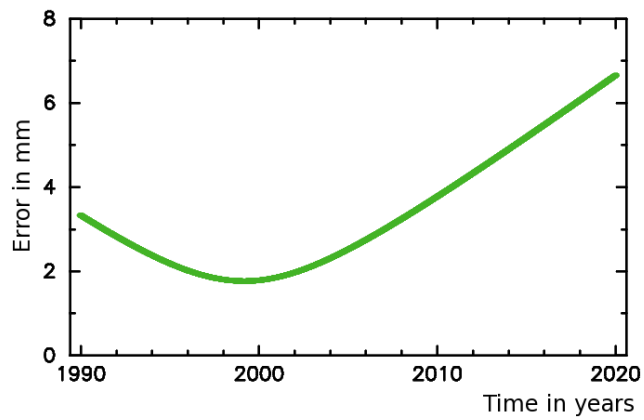

7 Conclusions

The observing campaign for monitoring the positions of the VLBA sites during 1994–2007 has been highly successful. The elements of the VLBA array during that period were determined with an accuracy of 2–3 mm in the vertical and in 0.4–0.6 mm for the horizontal component. This meets the requirements for position accuracy for astrometry and astrophysics programs at the VLBA.

The baseline length repeatability between the VLBA stations is smaller than that for the IVS non-VLBA stations. EOP estimates from the geodetic VLBA sessions are as close to GPS results as EOP estimates from the IVS sessions dedicated to precise EOP determination.

We found that the positions of all VLBA stations exhibit a significant seasonal signal with amplitudes of 1–8 mm in the vertical component and 0.5–3.5 mm in the horizontal component.

Several stations show anharmonic signals in their positions. We have traced the origin of these signals

to co-seismic deformations (MK-VLBA) and to a time-varying antenna tilt (PIETOWN). In the case of tilt, the signal can be successfully modeled using the pointing adjustment model, although the scaling factor between the antenna tilt and motion of the antenna reference point has to be determined from VLBI observations.

We have derived an empirical model of site motion that consists of linear velocity, a set of coefficients of the harmonic expansion and coefficients of the B-spline model that takes into account ad hoc motions. For the case where no ad hoc motion happens in the future, the accuracy of VLBA station position predictions would gradually degrade to 5–8 mm in the vertical and 1–1.5 mm in the horizontal component by the year 2020. However, unpredictable events, such as local deformations or post-seismic deformation could cause significantly greater errors. Therefore, continuation of VLBA site position monitoring is highly desirable.

Acknowledgements The National Radio Astronomy Observatory is a facility of the National Science Foundation operated under cooperative agreement by Associated Universities, Inc. We thank the staff of the VLBA for carrying these observations in their usual efficient manner. This work was done while J. Gipson, D. Gordon, D. MacMillan and L. Petrov worked for NVI, Inc. under NASA contract NAS5–01127.

References

Agnew, DC (1997) NLOADF: A program for computing ocean-tide loading, J Geophys Res, 102(B3):5109–5110

Beasley AJ, Gordron D, Peck AB, Petrov L, MacMillan DS, Fomalont EB, Ma C (2002) The VLBA Calibrator Survey–VCS1', Asrophys J Supp, 141:13–21, doi:10.1086/339806

Chock G (2006) Preliminary Observations on the Hawai'i Earthquakes of October 15, 2006, EERI Special Earthquake Report, Dec 2006

Hinteregger HF, Shapiro II, Robertson DC, Knight CA, Ergas RA, Whitney AA, Rogers AEE, Moran JM, Clark TA, Burke BF (1972) Precision Geodesy via Radio Interferometry, Science, 178:396-398, doi:10.1126/science.178.4059.396

Greisen EW (1988) Processing and Archiving of Astronomical Images. In: Acquisition, ed. Longo G & Sedmak G, Napoli: Osservatorio Astronomico di Capodimonte, 125

Kalnay EM, Kanamitsu M, Kistler R, Collins W, Deaven D, Gandin L, Iredell M, Saha S, White G, Woollen J, Zhu Y, Leetma A, Reynolds R, Chelliah M, Ebisuzaki W, Higgins W, Janowiak J, Mo KC, Ropelewski C, Wang J, Jenne R, Joseph D (1996) The NCEP/NCAR 40-Year Reanalysis Project, Bull Amer Meteorol Soc, 77:437–471

Kopeikin SM, Schäfer G (1999) Lorentz covariant theory of light propagation in gravitational fields of arbitrary-moving bodies, Phys Rev D, 60(12):124002, doi:10.1103/PhysRevD.60.124002

Kovalev YY, Lobanov AP, Pushkarev AB, & Zensus JA (2008) Opacity in compact extragalactic radio sources and its effect on astrophysical and astrometric studies, Astron & Astrophys, 483(3):759–768, doi:10.1051/0004-6361:20078679

Mathews PM (2001) Love numbers and gravimetric factors for diurnal tides, J Geod Soc Japan, 47(1):231–236

Matsumoto K, Takanezawa T, Ooe M (2000) Ocean tide models developed by assimilating TOPEX/POSEIDON altimeter data into hydrodynamical model: a global model and a regional model around Japan, J Oceanography, 56:567–581

Matveenko LI, Kardashev NS, & Sholomitsky GB (1965) On an interferometer with very long baseline, Izvestija Vysshih Uchebnyh Zavedenij, Radiofizika, 8:651–656

McCarthy DD and Petit G, Eds (2004) IERS Conventions 2003 IERS Technical Note, No. 32, Frankfurt am Main: Verlag des Bundesamts für Kartographie und Geodäsie

Napier PJ, Bagri DS, Clark BG, Rogers AEE, Romney JD, Thompson AR, Walker RC (1994) The Very Long Baseline Array, Proc IEEE, 82(5):658–671

Niell AE, (1996) Global mapping functions for the atmosphere delay at radio wavelengths, J Geophys Res, 100:3227–3246

Nothnagel A, Bromorzki O, Campbell J, Muskens A, Rottmann H, Rottman I (2002) Comparison of the Output of Repeated Mark III and Mark IV Correlation Results. In: IVS 2002 General Meeting Proceedings, ed Vandenberg N & Baver KD, 107–112

Petrov L, Ma C (2003), Study of harmonic site position variations determined by VLBI, J Geophys Res, 108(B4), 2190, doi: 10.1029/2002JB001801

Petrov L and Boy JP (2004) Study of the atmospheric pressure loading signal in VLBI observations, J Geophys Res, 109:B03405, doi:10.1029/2003JB002500

Petrov L (2007) The empirical Earth rotation model from VLBI observations, Astron & Astrophys, 467(1):359–369, doi:10.1051/0004-6361:20065091

Piner BG, Mahmud M, Fey AL, Gospodinova K (2007) Relativistic Jets in the Radio Reference Frame Image Database. I. Apparent Speeds from the First 5 Years of Data, Astron J, 133(5):2357–2388, doi:10.1086/514812

Ray RD (1999) A global ocean tide model from TOPEX/ POSEIDON altimetry: GOT99.2, NASA/TM-1999-209478, Greenbelt USA

Ray J and Altamimi Z (2005) Evaluation of co-location ties relating the VLBI and GPS reference frames, J. Geod, 79:189–185, doi:10.1007/s00190-005-0456-z

Saastamoinen J (1972) Contributions to the theory of atmospheric refraction, Bull Geod, 105:279–298

Saastamoinen J (1972) Introduction to practical computation of astronomical refraction. Part II Bull Geod, 106:383–397

Shapiro II, Knight CA (1970) Geophysical Applications of Long-Baseline Radio Interferometry. In: Earthquake Displacement Field and the Rotation of the Earth, ed. Beck A, Reidel, Dordecht, 284

Schlüter W, Behrend D (2007) The international VLBI service for geodesy and astrometry (IVS): current capabilities and future prospects, J Geod, 81(4–5):379–387, doi:10.1007/s00190-006-0131-z

Sovers OJ, Fanselow JL, Jacobs CS (1998) Astrometry and geodesy with radio interferometry: experiments, models, results, Rev Modern Phys, 70(4):1393–1454, doi:10.1103/RevModPhys.70.1393

Takahashi F, Kondo R, Takahashi Y, Koyama Y (2000) Very Long Baseline Interferometer, Ohmsha, Ltd, Tokyo

Thompson AR, Moran JM, Swenson GW (2001) Interferometry and synthesis in Radio astronomy, Wiley & Sons, Inc.

Walker RC (1999) Pointing Improvements Using Rail Height Information, VLBA Test Memo 61, National Radio Astronomy Observatory, Socorro, USA `http://www.vlba.nrao.edu/memos/test/test61memo.ps`